Wind Turbine Condition Monitoring based on an Improved Spline-Kernelled Chirplet Transform

***Abstract* — The time-varying operational conditions applied to wind turbines (WTs) not only challenge their operation but also make condition monitoring (CM) difficult. To achieve a reliable CM result, more advanced signal processing techniques, rather than the conventional spectral analyses, are urgently needed for interpreting the non-linear and non-stationary (NNS) CM signals collected from the turbines. The work presented in this paper is an effort for meeting such a requirement. Based on the proven capability of the Spline-kernelled Chirplet transform (SCT) in detecting the instantaneous frequencies (IF) within NNS mono-component signals, the paper improves the SCT to enable it to detect the instantaneous amplitude (IA) of lengthy NNS multi-component signals at a fault-related frequency of interest. The improved SCT is then applied for developing a new real-time CM technique dedicated to extracting fault-related features from WT CM signals. Experiment proves that the improved SCT has overcome existing SCT issues and is capable of correctly tracking the amplitude characteristics of NNS multi-component signals at fault-related frequencies of interest. The new CM technique developed, based on this improved SCT, shows success in detecting both mechanical and electrical faults occurring in a WT drive train, despite the constantly varying operational conditions of the turbine. Moreover, its algorithm is efficient in computation, which not only enables it to deal with lengthy NNS CM signals but makes it ideal for online use.**

Index Terms — wind turbine, condition monitoring, Chirplet transform.

I. Introduction

Wind turbines are power generation units exposed directly to a harsh environment, suffering time-varying loads and experiencing extreme operational temperature and humidity changes. They are therefore more prone to failure, in contrast to in-house generation units subject to fixed operational conditions [1],[2]. However, wind turbines (WTs) are usually deployed in remote land/water areas where access is difficult and their major operating components (e.g. blades, gearbox, generator, and power electronic converter) are placed at the top of a 70-100 m tower. All these features make the maintenance of WTs difficult, expensive and challenging. This is why remote condition monitoring (CM) has been strongly recommended in recent years by certificating bodies [3].

An efficient WT CM technique is expected to provide the operator with instant information about the health of the turbine to improve availability and therefore its economic return. In order to achieve such a technique considerable effort has been spent in the past decade. To date, various WT CM systems are available in the commercial market [4], and a variety of advanced WT CM techniques have been developed [5][6][7][8][9][10][11][12][13]. However, an agreed WT CM technique has not been achieved and false alarms are still frequently reported from site [14]. They not only increase the number of unnecessary site visits, prolonging downtime, but leave the turbine and its connections unsafe once a real fault occurs. Hence, improving the reliability of CM and reducing the chance of false alarms has become an urgent issue in the wind industry today. The root causes of these false alarms can be various, but the major ones are:

- Lack of an appropriate industry standard for WT CM;
- Lack of tools for correct interpretation of WT CM signals, which are non-linear & non-stationary (NNS) with time.

The first issue has been discussed in detail in [15]. This paper will be concentrated on a potential solution for the second issue.

To capture efficiently wind energy, most large modern WTs operate at variable speed. Accordingly, the CM signals collected from the WTs are characterized by NNS intra-wave features. The conventional Fourier transform (FT) analysis and its extension forms, e.g. bi-coherence [16] and side-band analysis [17], are unable to appropriately describe WT NNS signals, due to averaging, although spectral analyses are now being popularly adopted in some commercial WT CM systems [4][6][7]. To improve WT CM signal analysis efforts have been tried recently to investigate the potential of time-frequency analysis (TFA). For example, continuous wavelet transforms (CWTs) were applied to monitor WT blades in [18] and WT generators in [8][19][20]; Hilbert-Huang transforms (HHT) were used to detect WT mechanical faults in [21]; Short-time-Fourier transforms (STFT) were employed in [22] to monitor a WT induction generator; the S-transform was adopted for diagnosing WT gearbox failures in [23], and so on. These efforts promoted WT CM technology to certain extent. However, their commercial application is held back for the following reasons:

- Unsatisfactory time-frequency presentation of NNS signals, decreasing CM reliability.
  The STFT, wavelet transform and their combined S-transform adopt non-local adaption, which cannot show accurately non-linear features in an NNS signal, leading to energy leakage around the fault frequencies. This energy leakage accounts for smeared features and unidentified interference on the time-frequency map of the signal, decreasing signal interpretability and CM reliability.

- Complex TFA computing algorithms, whose lengthy operations hamper on-line, real-time CM.
  By contrast, the HHT uses locally adaptive calculations and decomposes the signal into a finite number of intrinsic mode functions (IMFs), describing non-linear signal features. However, the Empirical Mode Decomposition (EMD), used in HHT, is an automatic process, which is hard to adapt for on-line, real-time application in WT CM.
- Massive TFA calculation needs powerful computing hardware, increasing WT CM capital costs.
  Massive TFA calculations become more time-consuming and difficult when dealing with lengthy CM signals. This can be mitigated by improving computer hardware at the expense of CM capital cost. The WT operator then suffers a financial burden if each wind farm turbine has to be equipped with such a CM system.

The Chirplet transform (CT) [24] describes signals by using families of windowed chirp functions, which are related to one another by time-varying frequency or frequency-varying time modulations. Attributed to the closer geometric similarities, the chirp-like functions can describe better the non-linear 'intra-waves' in the NNS signals in contrast to the 'waves' and 'wavelets' of STFTs and CWTs respectively. Thus, in principle the CT has potential to provide more explicit description to the time-frequency features of the NNS WT CM signals. However, this application of CT to the field of WT CM has not been fully researched, although CT has been extensively applied in signal processing (e.g. [25][26]).

The CT relies on the application of a chirp kernel function, dominated by a parameter named the chirping rate. With the aid of a transform kernel, the time-frequency atoms of the CT can be shifted and sheared to suit the signal. Nonetheless, conventional CT fails to characterize non-linear frequency modulated signal's time-frequency features owing to its fixed chirping rate. To overcome this, a general chirplet chain method was proposed in [27], an adaptive CT was developed in [28], and another adaptive CT based on matching pursuit was studied in [29]. These studies assume the signal is the sum of a series of weighted chirplets and their residues and iteratively projects these residues into a predefined chirplet dictionary. In essence, they represent the signal using families of straight lines that fit the local energy ridge on the signal time-frequency map. However, the resultant broken lines cannot match the non-linear ridge curve very well.

To deal better with the signal with time varying instantaneous frequency (IF), the CT concept has been further developed recently. For example, Peng and his colleagues [30] proposed a general framework for parameterized time-frequency transforms, allowing various kinds of parameterized time frequency transforms, including the STFT and CT, to be constructed by selecting different kernel functions. Moreover, based on this framework they proposed three specific methods :

- The Polynomial CT (PCT) [31][32];
- The Generalized Warblet transform (GWT) [33];
- The Spline-kernelled CT (SCT) [34].

It has been proven that the SCT is more accurate than other methods when estimating the non-linearly varying IF of mono-component signals [34]. However, the SCT does not perform so well in detecting signal instantaneous amplitude (IA) at corresponding non-linearly varying IFs. Additionally, the SCT algorithm depicted in [34] is not applicable to multi-component signals. This defect significantly limits the extensive application of the SCT in engineering. One of the purposes of this paper is to fill these technology gaps by improving the SCT.

Additionally, despite the aforementioned achievements in the research of TFA methods, traditional FT-based spectral analyses are still popular in commercial WT CM systems although their disadvantages in dealing with NNS signals are widely reported [4]. This is because the real-time WT CM requires a CM system to extract CM features quickly from lengthy CM records, TFA methods are unable to meet such a requirement due to their complex calculations. Then, is it possible to develop an efficient algorithm to realize WT CM based on TFA? In the following, an efficient SCT-based CM tool will be developed dedicated to exploring such an approach.

II. THE SCT AND ITS IMPROVEMENT FOR ENERGY EXTRACTION FROM LENGTHY SIGNAL

According to [34], the SCT of a signal $x(t) \in \mathbf{L}^2(R)$ at $\tau \in (t_i, t_{i+1})$ is defined as

$$SCT(\tau, \omega, Q, \sigma) = \int_{-\infty}^{+\infty} \bar{z}(t) w_\sigma(t-\tau) e^{-j\omega t} dt \qquad (1)$$

with

$$\bar{z}(t) = z(t)\phi^R(t, Q)\phi^S(t, \tau, Q) \qquad (2)$$

where $z(t)$ is the analytical signal of $x(t)$, calculated through Hilbert transform $\mathbf{H}$, i.e. $z(t) = x(t) + j\mathbf{H}[x(t)]$. $\phi^R(t, Q)$ and $\phi^S(t, \tau, Q)$ are respectively the frequency-rotated and frequency-shifted operators, i.e.

$$\phi^R(t, Q) = e^{\Upsilon_i - j\sum_{k=1}^{n} q_k^i (t-t_i)^k/k} \qquad (3)$$

$$\phi^S(t, \tau, Q) = e^{j\sum_{k=1}^{n} q_k^i (\tau - t_i)^{k-1} t} \qquad (4)$$

where $Q(i,k) = q_k^i$ refers to the local polynomial coefficient matrix of the spline kernel, and Υ_i satisfies

$$\Upsilon_i - \Upsilon_{i+1} = \sum_{k=1}^{n} q_k^{i+1} (t_i - t_{i+1})^k / k \qquad (5)$$

with $\Upsilon_1 = 0$.

In [34] an effort was made to accurately extract mono-component IFs by optimizing the spline function, used to approximate the actual IF indicated by the energy ridge on the time-frequency map. However, from the point of view of CM, the extraction of Instantaneous Amplitude (IA) at the corresponding IF is more interesting because the variation of the CM signal amplitude at fault-related frequencies provides important CM clues and furthermore

aids damage assessment. Whether the SCT possesses similar comparable powerful IA detection capability to IF becomes a critical question. To answer this question, a mono-component signal with varying IF is simulated, i.e.

$$x(t) = \sin(2\pi\varphi(t)) \quad (0 \le t \le 10s) \tag{6}$$

with $\varphi(t) = 10t + 5\tan^{-1}(t-5)^2$.

From $\varphi(t)$, the IF of the signal can be inferred as

$$\omega(t) = 10 + \frac{10t-50}{1+(t-5)^4} \tag{7}$$

To facilitate understanding, both the time waveform and IF of the signal are shown in Fig.1.

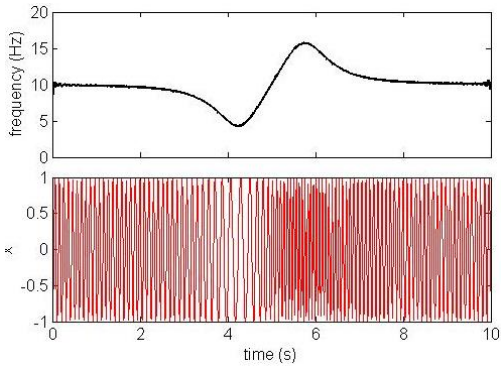

Fig.1 Signal depicted by (6).

From Fig.1, it is seen that the signal shows constant amplitude despite varying IF. SCT is then used to extract both the signal IF and IA as shown in Figs.2a and 2b. It is found that the SCT does show excellent capability in extracting the IF of the signal, through iterative optimization of the spline function. However, it fails to give a satisfactory description for the variation of the signal IA. The IA distortions at both boundaries are particularly significant. Such an issue discounts the added value of the SCT in signal processing, motivating the research of this paper to improve SCT.

The core idea for the improved SCT is to divide the original signal $x(t)$ into a number of time segments with the time span of τ. Hence, the original signal $x(t)$ can be expressed as

$$x(t) = \{X_{\tau,1} \quad X_{\tau,2} \quad \cdots \quad X_{\tau,i} \quad \cdots \quad X_{\tau,N-1} \quad X_{\tau,N}\} \tag{8}$$

where the subscript τ represents the time span of each segment, $i = 1,2,\cdots,N$ indicates the number of the segments in the sequence, and

$$N = fix\left(\frac{T}{\tau}\right) \tag{9}$$

$$\mathrm{T} = \frac{\mathrm{n}-1}{f} \tag{10}$$

$$X_{\tau,i} = \left\{x\left((i-1)\tau + \frac{1}{f}\right) \quad x\left((i-1)\tau + \frac{2}{f}\right) \quad \cdots \quad x(i\tau)\right\} \tag{11}$$

in which, T and f respectively denote the total time span and sampling frequency of the original signal, n refers to the number of data contained in the original signal.

Then, extract the IF and the change in the corresponding IA of every segment $x_{\tau,i}(t)$, taking full advantage of the SCT in IF extraction. Hereafter, 'the change of corresponding IA' will be simply described as 'IA' to be concise. Since the time span covering the signal segment is short, e.g. $\tau = 1s$ for all calculations presented in this paper, it is assumed that the IAs at both boundaries of the segment are similar to the average at the middle of the segment. The reason why time span $\tau = 1s$ will be explained in detail in next section. Based on that assumption we use that average IA to replace the IAs at both boundaries of the segment and then re-fit the modified IAs using a smooth spline curve. The data fitting result will be the new IAs for the present signal segment, i.e. $\mathrm{IA}_{\tau,i}(t)$. Accordingly, the sequential combination of all the new IA curves will be the IA for the whole signal, i.e.

$$\mathrm{IA(t)} = \{\mathrm{IA}_{\tau,1} \quad \mathrm{IA}_{\tau,2} \quad \cdots \quad \mathrm{IA}_{\tau,i} \quad \cdots \quad \mathrm{IA}_{\tau,N-1} \quad \mathrm{IA}_{\tau,N}\} \tag{12}$$

where

$$\mathrm{IA}_{\tau,i} = \left\{\mathrm{IA}\left((i-1)\tau + \frac{1}{f}\right) \quad \mathrm{IA}\left((i-1)\tau + \frac{2}{f}\right) \quad \cdots \quad \mathrm{IA}(i\tau)\right\} \tag{13}$$

To demonstrate the effectiveness of such a modified algorithm in improving the accuracy of IA extraction, the modified SCT algorithm was applied to extract both the IA and IF of the signal $x(t)$ as shown in Fig.2c.

(a)

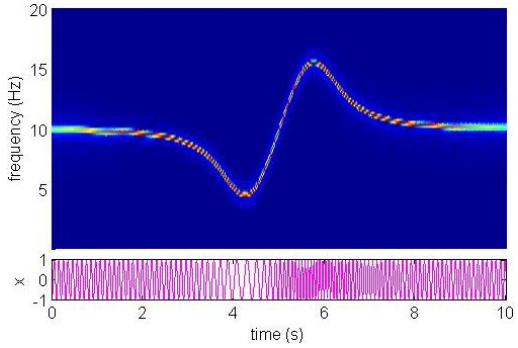

(b)

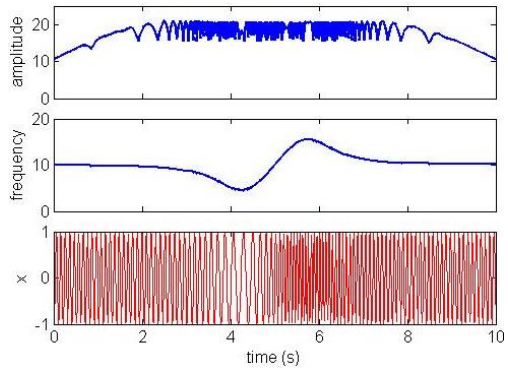

(c)

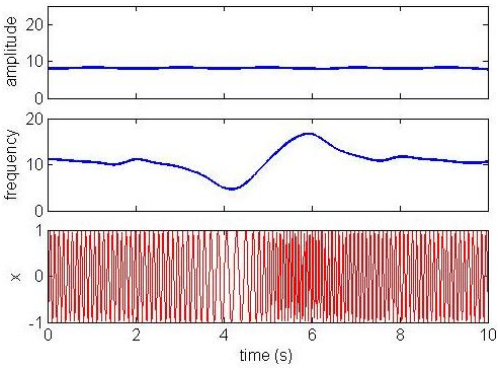

Fig.2 Results for the signal depicted by (6). (a) SCT map; (b) IA and IF by the SCT; (c) IA and IF by the improved SCT.

From Fig.2c, it is seen that the constant variation tendency of the IA of the signal has been correctly extracted thanks to the use of the improved SCT. In the meantime, it is noticed that a few distortions occur in the IF result due to the separate calculations of signal segments. But these distortions are tiny and can be ignored.

III. Further Improvement to the SCT for Wind Turbine Condition Monitoring

Since the improved SCT relies on dealing with the short signal segments we have avoided the necessity for processing lengthy data and do not require more powerful computer hardware, a desirable feature for WT CM. However, the improved SCT is still not applicable to WT CM until the following improvements are made to the algorithm.

Firstly, the improvement is made to enable the improved SCT to extract the IA and IF of multi-component signals, because all real WT CM signals are multi-component signals. Similar efforts have been reported in [35][36]. Unfortunately, the algorithms presented in both cannot be applied to WT CM because:

- Both algorithms were designed for detecting signal IFs and cannot guarantee the accuracy of the resultant IAs;
- Both algorithms require complex calculation, unsuitable for processing lengthy WT CM data.

For these reasons, an innovative approach has been developed as follows for adapting the improved SCT to extract the IA of a multi-component signal at fault-related frequencies of interest. It is well-known that for rotating machines, fault-related frequencies are functions of rotational speed. For example twice slip frequency indicates rotor winding faults in an induction machine [8]. In other words, the characteristic frequency of a certain type of fault can be predicted as long as the rotational speed of the machine is known. Therefore, a useful IA for the signal could be extracted at the characteristic fault-frequency using the following improved algorithms:

1) Purify the measured rotational speed

Fig.3 shows typical measured WT rotational speed data, which is always noisy. To calculate correctly the fault-related frequency so achieve an accurate prediction of IA that indicates the fault, it is necessary to purify the speed data. A time sliding window is designed for this purpose. The window length is dependent upon the data length, e.g. 1 second for all calculations presented in this paper. The sliding window is then moved forward along the signal and the average rotational speed at each time is calculated until the sliding window reaches the signal end. The overlap between consecutive movements relies on how frequently the speed fluctuates. In principle, the more frequent the speed fluctuation, the larger the overlap should be. In the end, a smooth spline is used to fit the average speed data to achieve the purified turbine rotational speed, as shown in Fig.3.

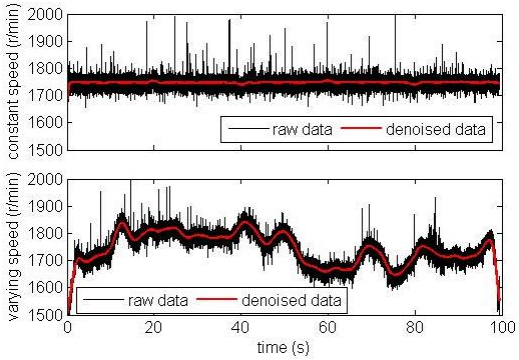

Fig.3 The purification of WT rotational speed data.

2) Calculate the fault-frequency of interest with the aid of the purified rotational speed

The fault-frequencies corresponding to various WT mechanical and electrical faults have been described in [2], they will not be repeated here to remain concise.

3) Extract the IA at the fault-frequency

To adapt the improved SCT for processing multi-component signals, it is essential to improve the IF extraction algorithm mentioned in [34]. Instead of optimizing the IF indicated by the energy ridge in the whole time-frequency plane, the improved SCT will optimize the IF indicated only by the energy ridge within a prescribed frequency band $[f-\Delta f, f+\Delta f]$. As Fig.4 shows, the frequency band will be centered at the fault-frequency of interest f, and its bandwidth is constant $2\Delta f$. The value of Δf is determined basically based on the distance between the frequency of interest and the frequencies in vicinity. In the calculations presented in the remaining part of this paper, a small value of Δf, i.e. $\Delta f = 2$ Hz, is selected in order to reduce computation burden and avoid the undesired influences by either noise or unidentified frequency components. As did in Section II, divide the original signal into a number of time segments first, and then iteratively apply the improved SCT to extracting the IAs of the signal segments at the frequency f until all signal segments are

processed. The energy variation of the signal at the fault-frequency will be exhibited by the combined IA curves.

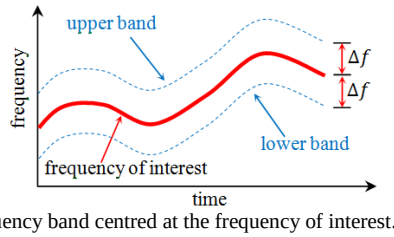

Fig.4 The frequency band centred at the frequency of interest.

It is worth noting here that the determination of the time segments is dependent on how rapidly WT speed fluctuates. In present WT control schemes the WT will not respond directly to a wind gust and WT rotational speed control relies on wind speed recorded from a low band-width anemometer filtered by the turbine controller, the SCADA system saves an average and standard deviation of wind speed every 10 minutes. The determination of time segments will be therefore based on this data. As depicted in [8], long-term WT 10 minutes SCADA data has shown wind speed fluctuations onshore of approximately 12~20%, whereas offshore the fluctuation is about 6%. For simplification, the authors assume the generator speed changes linearly with wind speed and consider the largest wind speed fluctuation to be 20% within 10 minutes. Then, for a generator speed 1600~1900 rev/min, as shown in Fig.3, its rotational frequency will vary 0.0080~0.0105 Hz per second, which can be considered negligible. Therefore each signal segment can be treated as linear and stationary if the CM signals are divided into a number of $1s$ segments, so $\tau = 1s$ is adopted in this paper.

Since fault alarms will be triggered by judging the IA of the CM signal at the fault-frequency, the DC components contained in the CM signal must be removed in advance for improving the reliability of CM. To reach such a purpose, a separate de-trending algorithm is developed dedicatedly for the improved SCT. As the improved SCT deals with the short signal segments that are approximately stationary along time, the FT is adopted for developing the algorithm. An illustrative example is given as follows:

Assume two signal pieces $x(t)$ and $x1(t)$, i.e.

$$\begin{cases} x(t) = 1 + \sin(2\pi f t) \\ x1(t) = \sin(2\pi f t) \end{cases} \quad (0 \le t \le 1s) \qquad (14)$$

with $f = 10\text{Hz}$.

A DC component is contained in signal $x(t)$, while there is no DC component in signals $x1(t)$. Their FT spectra are shown in Fig.5, and the first and last 10 of their FT coefficients are listed in Table 1. From both Fig.5 and Table 1, it is interestingly found that:

- the DC component in the signal only affects a limited number of FT coefficients locating at the beginning part of the FT spectrum, while it does not affect the ending FT coefficients;
- Table 1 shows that for both signals, the second FT coefficient is the conjugate of the last FT coefficient; the third FT coefficient is the conjugate of the second last coefficient, and so on.

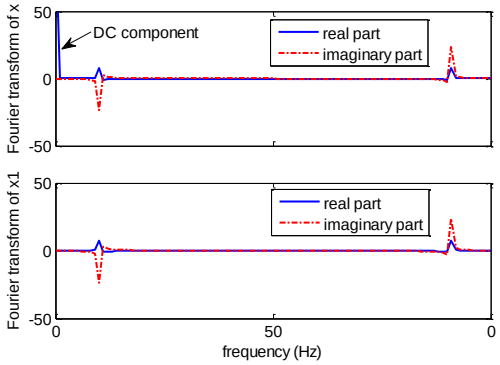

Fig.5 The FT spectra of the signals $x(t)$ and $x1(t)$.

Table.1 The first and last 10 FT coefficients of $x(t)$ and $x1(t)$

$\mathcal{F}(x)$				$\mathcal{F}(x1)$			
No.		**No.**		**No.**		**No.**	
1	101.0000	$N-10$		1	0.0000	$N-10$	
2	0.0000 + 0.0500i	$N-9$		2	0.0000 + 0.0500i	$N-9$	
3	0.0100 + 0.1000i	$N-8$	0.5900 - 2.0400i	3	0.0100 + 0.1000i	$N-8$	0.5900 - 2.0400i
4	0.0100 + 0.1600i	$N-7$	0.2600 - 1.0100i	4	0.0100 + 0.1600i	$N-7$	0.2600 - 1.0100i
5	0.0300 + 0.2300i	$N-6$	0.1400 - 0.6300i	5	0.0300 + 0.2300i	$N-6$	0.1400 - 0.6300i
6	0.0500 + 0.3100i	$N-5$	0.0800 - 0.4400i	6	0.0500 + 0.3100i	$N-5$	0.0800 - 0.4400i
7	0.0800 + 0.4400i	$N-4$	0.0500 - 0.3100i	7	0.0800 + 0.4400i	$N-4$	0.0500 - 0.3100i
8	0.1400 + 0.6300i	$N-3$	0.0300 - 0.2300i	8	0.1400 + 0.6300i	$N-3$	0.0300 - 0.2300i
9	0.2600 + 1.0100i	$N-2$	0.0100 - 0.1600i	9	0.2600 + 1.0100i	$N-2$	0.0100 - 0.1600i
10	0.5900 + 2.0400i	$N-1$	0.0100- 0.1000i	10	0.5900 + 2.0400i	$N-1$	0.0100 - 0.1000i
11		N	0.0000 - 0.0500i	11		N	0.0000 - 0.0500i

These findings inspire a simple de-trending algorithm for the improved SCT, i.e.

a) Perform the FT of the signal segment being considered;
b) Set the first FT coefficient to be zero and replace the other starting FT coefficients with the conjugates of the corresponding ending FT coefficients to ensure a minimized DC component effect;
c) Implement the inverse FT of the modified FT coefficients to obtain the expected de-trended signal segment.

To verify the effectiveness of above improvements, a non-stationary multi-component signal is simulated. It is formulated as follows:

$$x(t) = \begin{cases} \sin(2\pi f_1 t) & (0 \le t \le 1s) \\ 2 + 2\sin(2\pi f_2 t) & (1 < t \le 2s) \\ \sin(2\pi f_1 t) + 3\sin(2\pi f_2 t) - 2 & (2 < t \le 3s) \\ 5 + 2\sin(2\pi f_1 t) + \sin(2\pi f_2 t) + \sin(2\pi f_3 t) & (3 < t \le 4s) \end{cases} \qquad (15)$$

with $f_1 = 80\text{Hz}$, $f_2 = 30\text{Hz}$, and $f_3 = 50\text{Hz}$.

First of all, the conventional CT was applied to the signal in order to have a basic understanding of the time-frequency feature of the signal as shown in Fig.6a. But unfortunately, it is very difficult to perceive the wanted information from the CT map. Thus, the improved SCT was applied to extract the IAs of the signal at frequencies f_1, f_2 and f_3. The results are shown in Fig.6b.

(a)

(b)

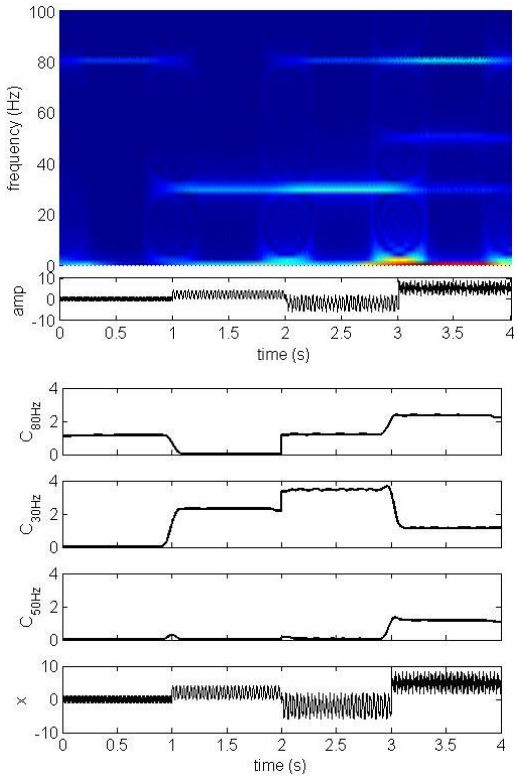

Fig.6 Verification of the improved SCT. (a) Time-frequency map by the conventional CT; (b) Extracted IAs at the frequencies of interest by the improved SCT.

From Fig.6b, it is seen that the variation tendencies of the amplitudes at the three characteristic frequencies have been extracted correctly by using the improved SCT despite the time varying 'multi-component' features and the disturbance of DC components. It is worth noting that the IAs shown in Fig.6b have been calibrated using the SCT coefficients for a unit amplitude harmonic signal (i.e. the signal presented in the first time segment), so the extracted IA value can approximate to the actual frequency component amplitudes. But this is not always required in the practice of machine CM.

IV. Application of the Improved SCT to Wind Turbine Condition Monitoring

To demonstrate the potential of the improved SCT in WT CM, the improved SCT has been applied to the CM signals collected from a WT drive train test rig, reported in [8]. As Fig.7a shows, the test rig compromises a 54 kW DC variable-speed motor, a two-stage gearbox with the gear ratio of 5:1, and a three-phase 4-pole wound-rotor induction generator that was rated for the experiment at 30 kW. The rotor circuit of the generator is coupled via slip rings to an external three-phase resistive load bank, so that electrical imbalance can be applied to the generator rotor. The test rig was instrumented and controlled using LabVIEW. In the experiments, various wind speed inputs were applied to the test rig via the DC motor, the speed of which was controlled by an external model incorporating the properties of a 2 megawatt WT operating under closed-loop conditions, driven by natural wind at a variety of speeds and turbulences. For this research, both generator electrical imbalance and shaft mechanical unbalance were emulated on the test rig. The relevant CM signals were collected from the terminals of the generator and its input-side shaft by using a sampling frequency of 1 kHz, see Fig.7b.

(a)

(b)

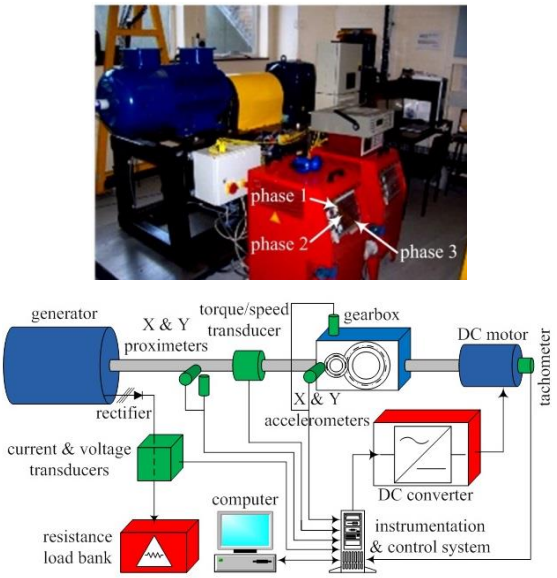

Fig.7 WT drive train test rig. (a) Front view; (b) Schematic diagram.

In the experiments, a generator rotor winding fault was emulated first on the test rig by changing the phase resistances of the load bank. To observe the effect of the fault, two large rotor asymmetries, i.e. $U_e = 30\%$ from 20s to 40s and $U_e = 15\%$ from 60s to 80s, were first applied to the generator. The method for assessing electrical asymmetry U_e has been depicted in [8]. When the test rig operated at variable speeds, the output power of the generator and its time-frequency analysis result by the conventional CT are shown in Fig.8.

From Fig.8 the conventional CT had difficulty providing explicit time-frequency features of the signal. However, the fault-induced characteristics at the twice slip frequency $2sf_s$ of the generator can be clearly observed when the electrical asymmetries are applied to the generator rotor. Herein, s refers to induction machine slip and f_s indicates the electrical supply frequency. Since when the rotor phase resistances are imbalanced, the generator current, voltage, and power are modulated at twice the slip frequency as the rotor asymmetry moves through the air gap magnetic field twice for every pole pair cycle, the twice slip frequency $2sf_s$ is usually regarded as the characteristic frequency for

diagnosing the generator rotor winding fault [8]. To extract this fault-induced characteristic, the improved SCT was applied to the power signal in Fig.8 and the result is shown in Fig.9.

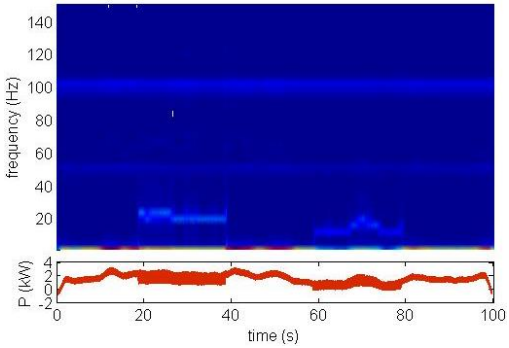

Fig.8 Power signal collected at variable rotational speed and its time-frequency map by the conventional CT.

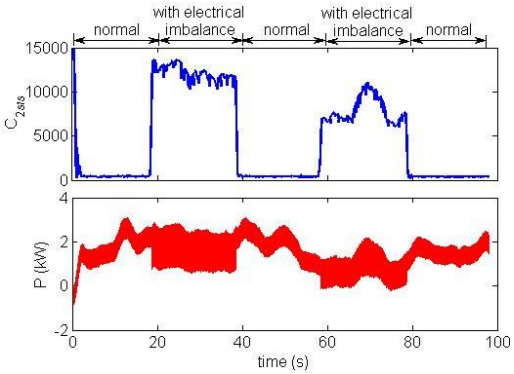

Fig.9 The improved SCT result for the power signal in Fig.8.

Based on the result shown in Fig.9, it can be concluded that the improved SCT can successfully predict the presence of the fault. To verify the effectiveness of the improved SCT in incipient fault detection, two small levels of rotor asymmetries, i.e. $U_e = 4.7\%$ from 60s to 120s and $U_e = 9.2\%$ from 180s to 240s, were applied to the generator through the resistive load bank. The corresponding power signal feature extraction result by the improved SCT is shown in Fig.10.

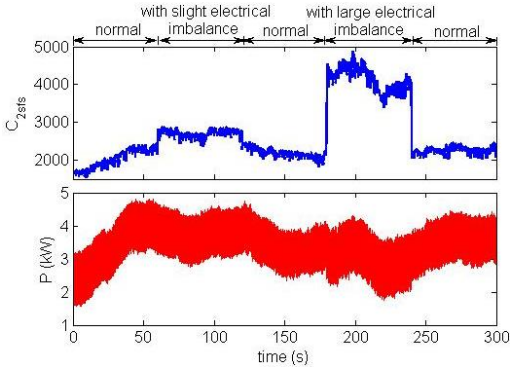

Fig.10 The improved SCT result for the power signal collected when different severity levels of rotor imbalance faults were emulated.

From Fig.10, it is seen that both the incipient and the early developed electrical imbalance faults have been detected successfully by the improved SCT despite the significantly varying generator speed and large electrical power fluctuation.

Following the successful detection of the electrical fault, the CM capability of the improved SCT in detecting a WT mechanical fault was also verified on the test rig. The experimental set-up for emulating mechanical fault is shown in Fig.11, where, two unbalance masses were installed on the input-side shaft of the generator to create a desired shaft unbalance with balance quality grade $G = 13.9$ mm/s [37], which was assessed based on the British and International Standard BS ISO 1940-1 [38]. As the practice reported in [8][20][39][40] has shown that the mechanical fault occurring in WT drive train can also be detected through analysing the electrical signals measured from the terminals of WT generator, both the shaft vibration and electrical power signals of the generator were collected when the test rig operated at varying speeds. The time waveforms of both are shown in Fig.12.

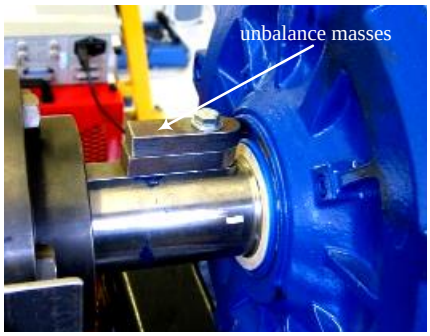

Fig.11 Experimental set-up for emulating shaft unbalance fault.

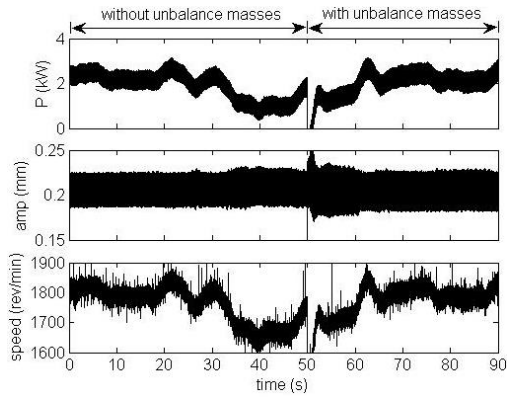

Fig.12 The CM signals collected when shaft mechanical unbalance fault was emulated on the test rig.

From Fig.12, it is found that the power signal was dominated by the generator speed from which nothing about the fault can be perceived. By contrast, the shaft vibration signal is less affected by speed. Moreover, its amplitude gives an indication of the fault, although the indication is not sufficiently self-evident to be adopted as a valid proof of fault.

To detect this mechanical fault, both the shaft vibration signal and the power signal were interpreted by using the improved SCT. Firstly, the IA of both signals at the shaft

rotational frequency, i.e. C_{rpm}, was extracted as shown in Fig.13. Herein, the IA at shaft rotating frequency is interested because the shaft rotating frequency is the characteristic frequency of a mechanical shaft unbalance fault.

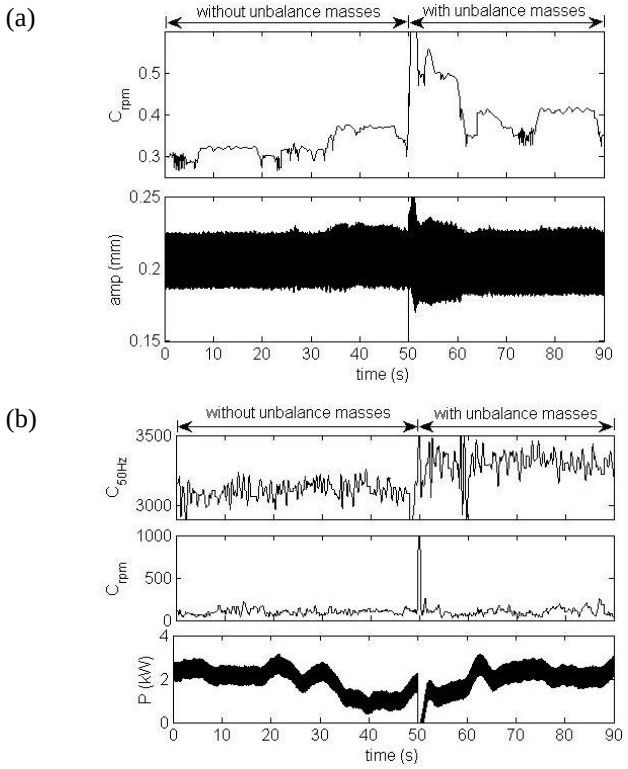

Fig.13 Detect mechanical fault using the improved SCT. (a) Interpretation of mechanical signal; (b) Interpretation of electrical power signal.

From Fig.13, it is found that as expected, the resultant C_{rpm} derived from the shaft vibration signal shows a general increase in the presence of the fault. However, the tendency is not explicit enough to support a firm CM conclusion. In comparison, the C_{rpm} extracted from the power signal does not show any interesting difference in value before and after the application of the unbalance. This suggests that the application of the unbalance masses does not have sufficient influence on the generator dynamic eccentricity because of a short, stiff rotor shaft. It is well known that a mechanical fault occurring in shaft, e.g. shaft unbalance fault in this experiment, will disturb the torque delivered by the shaft. Since power is the product of shaft torque and its rotating frequency, the generator power will be influenced too as a consequence of the mechanical fault [8, 20]. As the electric power output from an induction generator is dominated by the three-phase electric currents and voltages at nominal frequency (mains frequency is 50Hz in Europe and 60Hz in America), the IA of the electric signals at nominal frequency will respond once a mechanical fault is present in the WT drive train [2, 41]. For this reason, the IA of the generator power signal at the nominal frequency of 50 Hz, i.e. C_{50Hz}, was extracted using the improved SCT. The result is also plotted in Fig.13b. Obviously, the resultant C_{50Hz} provides a more convincing proof of the presence of the shaft unbalance fault in contrast to C_{rpm}.

All the aforementioned calculations were performed in a computer with 3.30GHz of Intel Pentium processor and 16GB of RAM. To demonstrate the excellent computational efficiency of the improved SCT in comparison to the conventional SCT, the time taken by both algorithms for processing the electric power signals *P* in Figs. 9, 10 and 13 are listed in Table 2.

From Table 2, it is seen that the time taken by the improved SCT is generally less than half of that taken by the conventional SCT. Thus, it can be concluded that the improved SCT is much more computationally efficient than the conventional SCT and therefore more ideal for online use.

Table.2 Computational efficiency comparison between the improved and conventional SCT.

Electric power signal *P*	**Time Cost** (s)	
	Improved SCT	**Conventional SCT**
In Fig.9	39	62
In Fig.10	135	276
In Fig.13	57	135

V. CONCLUSIONS

To improve WT CM technology for analysing lengthy NNS WT CM signals, a new WT CM technique is proposed in this paper, based on improving the SCT.

From this research, it can be concluded that the improved SCT has shown great success in extracting the IA of lengthy NNS multi-component signals at the fault-frequencies of interest from a test rig. Moreover, with the aid of the purified WT rotational speed, the improved SCT provides a powerful tool for interpreting NNS WT CM signals. Experiment shows that the CM technique based on the improved SCT is capable of detecting both the mechanical and electrical faults occurring in the WT despite its constantly varying load. In addition, thanks to the efficient computational algorithm of the improved SCT, accurate analysis of lengthy WT CM signals does not require more costly WT CM hardware. Thus, it is recommended that the improved SCT is feasible for a new generation of high quality CM WT systems.

In view of this, further work will be done to continue to verify the capability of the improved SCT for detecting a wider range of WT faults on operating WTs to make it ready for commercial exploitation.

REFERENCES

[1] J. Ribrant and L. Bertling, "Survey of failures in wind power systems with focus on Swedish wind power plants during 1997-2005," *IEEE Trans. Energy Convers.*, vol.22, no.1, pp 167-173, 2007.

[2] P. Tavner, *Offshore Wind Turbine: Reliability, Availability & Maintenance*. IET Press, ISBN: 978-1-84919-229-3, 2012.

[3] DNV GL, *Guideline for the certification of condition monitoring systems for wind turbines*, Edition 2013.

[4] W. Yang, P. Tavner, C. Crabtree, Y. Feng, and Y. Qiu, "Wind turbine condition monitoring: technical and commercial challenges," *Wind Energy*, vol.17, no.5, pp 673-693, 2014.

[5] P. Caselitz and J. Giebhardt, "Rotor condition monitoring for improved operational safety of offshore wind energy converters," *Trans. ASME, J. Sol. Energy Eng.*, vol.127, pp 253-261, 2005.

[6] C.C. Ciang, J.R. Lee, and H.J. Bang, "Structural health monitoring for a wind turbine system: a review of damage detection methods," *Meas. Sci. Technol.*, vol.19, pp 1–20, 2008.

[7] Y. Amirat, M.E.H. Benbouzid, E. Al-Ahmar, B. Bensaker, and S. Turri, "A brief status on condition monitoring and fault diagnosis in wind energy conversion systems," *Renew. Sustain. Energy Rev.*, vol.13, pp 2629–2636, 2009.

[8] W. Yang, P. Tavner, C. Crabtree, and M. Wilkinson, "Cost-effective condition monitoring for wind turbines," *IEEE Trans. Ind. Electron.*, vol.57, no.1, pp 263-271, 2010.

[9] B. Lu, Y. Li, X. Wu, and Z. Yang, "A review of recent advances in wind turbine condition monitoring and fault diagnosis," in *Proc. IEEE Power Electron. Mach. Wind Appl. (PEMWA)*, Lincoln, June 2009.

[10] Y. Da, X. Shi, and M. Krishnamurthy, "A new approach to fault diagnostics for permanent magnet synchronous machines using electromagnetic signature analysis," *IEEE Trans. Power Electron.*, vol.28, no. 8, pp 4104-4112, 2013.

[11] A. Hamilton, A. Cleary, and F. Quail, "Development of a novel wear detection system for wind turbine gearboxes," *IEEE Sensors J.*, vol.14, no.2, pp 465-473, 2014.

[12] N. Freire, J. Estima, and A. Marques Cardoso, "Open-circuit fault diagnosis in PMSG drives for wind turbine applications," *IEEE Trans. Ind. Electron.*, vol.60, no.9, pp 3957-3967, 2013.

[13] J.-Y. Park, J.-K. Lee, K.-Y. Oh, and J.-S. Lee, "Development of a novel power curve monitoring method for wind turbines and its field tests," *IEEE Trans. Energy Convers.*, vol.29, no.1, pp 119-128, 2014.

[14] Y. Qiu, Y. Feng, P. Tavner, P. Richardson, G. Erdos, and B. Chen, "Wind turbine SCADA alarm analysis for improving reliability," *Wind Energy*, vol.15, no.8, pp 951-966, 2012.

[15] W. Yang and R. Court, "Experimental study on the optimum time for conducting bearing maintenance," *Meas.*, vol.46, no. 8, pp 2781-2791, 2013.

[16] W. Jeffries, J. Chambers, and D. Infield, "Experience with bicoherence of electrical power for condition monitoring of wind turbine blades," *IEE Proc. Vis. Image Signal Pro.*, vol. 145, no.3, pp 141-148, 1998.

[17] D. Zappalá, P. Tavner, C. Crabtree, and S. Sheng, "Side-band algorithm for automatic wind turbine gearbox fault detection and diagnosis," *IET Renew. Power Gen.*, vol. 8, no. 4, pp 380-389, 2014.

[18] C. Tsai, C. Hsieh, and S. Huang, "Enhancement of damage-detection of wind turbine blades via CWT-based approaches," *IEEE Trans. Energy Convers.*, vol.21, no.3, pp 776-781, 2006.

[19] S. Watson, B. Xiang, W. Yang, P. Tavner, and C. Crabtree, "Condition monitoring of the power output of wind turbine generators using Wavelets," *IEEE Trans. Energy Convers.*, vol.25, no.3, pp 715-721, 2010.

[20] W. Yang, P. Tavner, and M. Wilkinson, "Condition monitoring and fault diagnosis of a wind turbine synchronous generator drive train," *IET Renew. Power Gen.*, vol.3, no.1, pp 1-11, 2009.

[21] D. Lu, W. Qiao, X. Gong, and L. Qu, "Current-based fault detection for wind turbine systems via Hilbert-huang transform," *IEEE Power and Energy Society General Meeting* (PES), pp 1-5, Vancouver, Canada, 21-25 July, 2013.

[22] C. Crabtree, S. Djurovic, P. Tavner, and A. Smith, "Fault frequency tracking during transient operation of wind turbine generators," *2010 XIX International Conference on Electrical Machines* (ICEM), pp 1-5, Rome, Italy, 6-8 September 2010.

[23] W. Yang, L. Christian, and R. Court, "S-transform and its contribution to wind turbine condition monitoring," *Renew. Energy*, vol.62, pp 137-146, 2014.

[24] S. Mann and S. Haykin, "The chirplet transform: Physical considerations," *IEEE Trans. Signal Process.*, vol.43, no.11, pp 2745-2761, 1995.

[25] F. Millioz and M. Davies, "Sparse detection in the chirplet transform: application to FMCW radar signals," *IEEE Trans. Signal Process.*, vol.60, no.6, pp 2800-2813, 2012.

[26] J. Cui and W. Wong, "Investigation of short-term changes in visual evoked potentials with windowed adaptive chirplet transform," *IEEE Trans. Biomed. Eng.*, vol.55, no.4, pp 1449-1454, 2008.

[27] E. Chassande-Mottin and A. Pai, "Best chirplet chain: Near-optimal detection of gravitational wave chirps," *Phys. Rev. D.*, vol.73, no.4, pp 42003-42026, 2006.

[28] D. Mihovilovic and R. Bracewell, "Adaptive chirplet representation of signals on time-frequency plane," *Electron. Lett.*, vol.27, no.13, pp 1159-1161, 1991.

[29] J. Cui and W. Wong, "The adaptive chirplet transform and visual evoked potentials," *IEEE Trans. Biomed. Eng.*, vol.53, no.7, pp 1378-1384, 2006.

[30] Y. Yang, Z. Peng, X. Dong, W. Zhang and G. Meng, "General parameterized time-frequency transform," *IEEE Trans. Signal Process.*, vol.62, no.11, pp 2751-2764, 2014.

[31] Z. Peng, G. Meng, F. Chu, Z. Lang, W. Zhang, and Y. Yang, "Polynomial chirplet transform with application to instantaneous frequency estimation," *IEEE Trans. Instrum. Meas.*, vol.60, no.9, pp 3222-3229, 2011.

[32] Y. Yang, Z. Peng, W. Zhang, and G. Meng, "Frequency-varying group delay estimation using frequency domain polynomial chirplet transform," *Mech. Syst. Signal Process.*, vol.46, no. 1, pp 146-162, 2014.

[33] Y. Yang, Z. Peng, G. Meng, and W. Zhang, "Characterize highly oscillating frequency modulation using generalized warblet transform," *Mech. Syst. Signal Process.*, vol.25, pp 128-140, 2012.

[34] Y. Yang, Z. Peng, G. Meng, and W. Zhang, "Spline-kernelled chirplet transform for the analysis of signals with time-varying frequency and its application," *IEEE Trans. Ind. Electron.*, vol.59, no.3, pp 1612-1621, 2012.

[35] Y. Yang, W. Zhang, Z. Peng, and G. Meng, "Multicomponent signal analysis based on polynomial chirplet transform," *IEEE Trans. Ind. Electron.*, vol.60, no.9, pp 3948-3956, 2013.

[36] Y. Yang, Z. Peng, X. Dong, W. Zhang, and G. Meng, "Application of parameterized time-frequency analysis on multicomponent frequency modulated signals," *IEEE Trans. Instrum. Meas.*, vol.63, no.12, pp 3169-3180, 2014.

[37] W. Yang, R. Court, P. Tavner, and C. Crabtree, "Bivariate empirical mode decomposition and its contribution to wind turbine condition monitoring," *J. Sound Vib.*, vol.330, pp 3766-3782, 2011.

[38] *Mechanical Vibration – Balance quality requirements for rotors in a constant (rigid) state – Part 1: Specification and verification of balances. ISO 1940-1: 2003*, International Organization for Standardization, Geneva, Switzerland, 2003.

[39] X. Gong and W. Qiao, "Bearing fault diagnosis for direct-drive wind turbines via current demodulated signals," *IEEE Trans. Ind. Electron.*, vol. 60, no. 8, pp 3419-3428, 2013.

[40] X. Gong and W. Qiao, "Current-based mechanical fault detection for direct-drive wind turbines via synchronous sampling and impulse detection," *IEEE Trans. Ind. Electron.*, vol.62, no.3, pp 1693-1702, 2015.

[41] P. Tavner, "Review of condition monitoring of rotating electrical machines," *IET Electr. Power Appl.*, vol.2, no.4, pp 215-247, 2008.